J. Fluid Mech. (1995), *vol.* 283, *pp.* 175–200

Deformation of liquid capsules with incompressible interfaces in simple shear flow

By HUA ZHOU AND C. POZRIKIDIS

Department of Applied Mechanics and Engineering Sciences, University of California at San Diego, La Jolla, CA 92093-0411, USA

(Received 15 October 1993 and in revised form 9 August 1994)

The transient deformation of liquid capsules enclosed by incompressible membranes whose mechanical properties are dominated by isotropic tension is studied as a model of red blood cell deformation in simple shear flow. The problem is formulated in terms of an integral equation for the distribution of the tension over the cell membrane which is solved using a point-wise collocation and a spectral-projection method. The computations illustrate the dependence of the deformed steady cell shape, membrane tank-treading frequency, membrane tension, and rheological properties of a dilute suspension, on the undeformed cell shape. The general features of the evolution of two-dimensional cells are found to be similar to those of three-dimensional cells, and the corresponding membrane tank-treading frequency and maximum tension are seen to attain comparable values. The numerical results are compared with previous asymptotic analyses for small deformations and available experimental observations, with satisfactory agreement. An estimate of the maximum shear stress for membrane breakup and red blood cell hemolysis is deduced on the basis of the computed maximum membrane tension at steady state.

1. Introduction

The deformation of erythrocytes, also called red blood cells, is an important field of study in biorheology and a significant area of clinical and laboratory blood research. Interest in the topic within the discipline of fluid dynamics has arisen simultaneously with the realization that red blood cells are nucleus-free capsules that are enclosed by a biological membrane with a composite structure and unusual mechanical properties (Dintenfass 1962). This feature distinguishes the behaviour of red blood cells from that of inflexible rigid particles or deformable liquid droplets with regular interfaces characterized by isotropic surface tension. The internal fluid of the red blood cells is an aqueous solution of hemoglobin which, under normal conditions, may be considered to be a Newtonian fluid. In the absence of an external flow, healthy red blood cells assume the shape of biconcave disks with a range of aspect ratios.

A satisfactory understanding of the structure of the cell membrane is now believed to be available. The membrane is known to consist of a double layer of similar but not identical lipids that face away from each other and rest against the cell skeleton. The latter is a network of the extrinsic protein spectrin, held together by linking actin filaments and protein 4.1. Other intrinsic proteinic molecules transverse the arrangement of the lipid molecules and serve to anchor the skeleton onto the bi-layer (Evans & Skalak 1980; Fischer 1992). It has been shown that the membrane has a fluid-like character as manifested by the diffusion of surface tracers, and a solid-like character as manifested by the fact that the cell returns to its unstressed shape after

deformation. It is not clear, however, whether material particles on the membrane assume their original relative position after the cell has returned to the unstressed state.

Certain aspects of the mechanical properties of the cell membrane have been established with confidence, but a satisfactory mechanical model applicable to arbitrary deformations is not available (Tözeren *et al.* 1984). One well-established property is that the surface area of the membrane is locally and globally conserved, which means that a differential material element of the membrane maintains its original surface area. Another well-established property is that the membrane exhibits some type of viscoelastic behaviour (Skalak, Özkaya & Skalak 1989). The membrane incompressibility and viscous behaviour are attributed to the lipid bi-layer, whereas the elastic behaviour is attributed to the spectrin skeleton. The values of the effective rheological constants of the membrane depend upon the cell's health and age, but also upon the history, severity, and type of deformation (Sutera, Mueller & Zahalak 1990). Structural rearrangements in the network of the intrinsic proteins at large deformations may be responsible for plastic behaviour.

The effect of the membrane mechanical properties on the cell's mobility and deformation in an applied flow is a central issue in the study of blood flow. A stiff membrane or a membrane with a reduced surface area yields a cell that is difficult to deform and more likely to occlude the entries of capillaries, thereby causing several types of blood pathology including sickle cell anemia, cerebral malaria, and possibly diabetes (Sutera & Krogstad 1991). To develop a treatment, it is important to establish the relationship between the membrane's chemical composition and mechanical properties so that the cell motion may be monitored and thus controlled.

A great deal of our current understanding of the behaviour of red blood cells in flow is due to experimental observations of the cells' deformation in unidirectional simple shear flow. Schmid-Schönbein & Wells (1969) and Goldsmith (1971) were the first to demonstrate that red blood cells in simple shear flow exhibit two types of motion: rotation like rigid particles at low shear rates, and a fluid drop-like motion and deformation at higher shear rates. In the latter type of motion the dimples of the biconcave disk disappear and the cell assumes the shape of a prolate ellipsoid, while the membrane rotates like a tank tread around the cytoplasmic fluid. Subsequent research has shown that the ratio of viscosities between the suspending and cytoplasmic fluid may play an important role in demarcating the prevailing type of behaviour, rotation versus deformation along a stationary axis (Goldsmith & Marlow 1972; Keller & Skalak 1982).

In carrying out theoretical and computational studies of red blood cell deformation due to flow, a mechanical model of the cell membrane must be adopted; and since a complete understanding of the membrane's mechanical response is not available, some approximations must be introduced. A viscoelastic model that incorporates an effective surface viscosity and moduli of elasticity is considered to be adequate for small deformations, although care must be taken so that the condition of membrane incompressibility is not violated at a significant level (Evans & Hochmuth 1976; Evans & Skalak 1980).

In the present work we perform a computational study of red blood cell deformation in simple shear flow, maintaining the condition of membrane incompressibility and neglecting the viscoelastic behaviour. Specifically, we assume that the cell membrane is a thin shell that supports isotropic tension and, thus, it behaves like a two-dimensional inviscid fluid with the tension playing the role of surface pressure. In the mathematical formulation, the tension is an unknown which is to be computed as part of the solution so as to satisfy the condition of incompressibility, that is, so as to ensure that the

surface area of an arbitrary element of the membrane is conserved during the motion. The model of incompressible surface flow may be readily combined with a viscoelastic model to yield a more realistic description of the cell's behaviour, but this results in a numerical problem that is intractable with the currently available computational resources (Pozrikidis 1994, 1995).

One important consequence of neglecting the elastic behaviour is that if the flow is stopped, the cell will not return to the unstressed shape of the biconcave disk but will retain its instantaneous configuration. Another consequence is that the stationary deformed cell shape depends only upon the membrane surface area and is independent of the shear rate and of the initial cell configuration, as long as the latter is not substantially involved. Thus, differences in the asymptotic shapes corresponding to different initial cell shapes and orientations are due to numerical error. Fischer (1980) reported that the energy dissipation within the membrane is higher than or comparable to that in the cytoplasm for a wide range of shear rates, and the steady cell shapes show some dependence on the shear rate. These observations underline the limitations of the present model.

The present study is based on numerical solutions of a series of initial value problems in which a two-dimensional or three-dimensional cell deforms from a specified initial shape until it reaches a steady state. The numerical procedure is based on a variation of the boundary integral method which formulates the problem in terms of an integral equation of a non-standard type over the cell surface. One distinguishing feature of the present study is that the computations follow the cell motion at large deformations. The results of the three-dimensional computations depart from those of previous studies for two-dimensional or axisymmetric flows, and represent a first attempt to describe cell behaviour in a genuinely three-dimensional flow.

One objective of the present computations is to estimate the membrane tension and tank-treading frequency as functions of the initial cell shape. These results are useful in establishing thresholds for the maximum shear stress or shear rate above which the membrane is expected to fail. The thresholds are derived on the assumption that the membrane fails at a specified level of tension that must be found by laboratory observation, neglecting the effect of membrane fatigue due to cyclic loading associated with ageing. The results for the cell shape are used to compute the effective viscosity and normal-stress differences of a dilute suspension using a well-established formalism that was originally developed for suspensions of liquid droplets. The contribution of the membrane viscous dissipation to the effective stress tensor is taken into consideration.

To make the computations tractable, we shall assume that the viscosity of the cytoplasmic fluid is equal to that of the suspending fluid. Under normal conditions *in vivo*, the viscosity ratio between these two fluids is close to five, but experiments *in vitro* are usually conducted using a dextran–saline solution as the suspending medium and therefore in a range of viscosity ratios including the value of unity. Keller & Skalak (1982) showed that the viscosity ratio plays an important role in determining the character of the asymptotic motion, and predict that, when the viscosity ratio is equal to one, the cell deforms to a steady asymptotic shape. When steady tank-tread motion is established, the tank-treading frequency of red blood cells is known to be insensitive to the viscosity of the suspending medium (Fischer, Stöhr-Liesen & Schmid-Schönbein 1978).

There are a number of previous analytical and computational studies of the behaviour of red blood cells in simple shear flow and we review certain salient contributions. One class of studies has considered the behaviour of two-dimensional

cells bounded by incompressible membranes. Kholeif & Weymann (1974) computed the motion of cells whose cross-sectional shape is given by the Cassini ovals, and observed that the cell may either rotate as a rigid particle or exhibit steady deformation similar to that of liquid droplets (Stone 1994). The prevailing behaviour was found to depend upon the magnitude of the membrane tank-treading velocity which was a free parameter of their problem. Sugihara & Niimi (1984) and Niimi & Sugihara (1985) considered the corresponding behaviour of cells with elliptical shapes and computed the membrane tension and time of exposure to high tension. One objective of their studies was to identify conditions for material fatigue leading to membrane breakup. Zahalak, Rao & Sutera (1987) relaxed the assumption of fixed particle shape and solved for the steady shapes of two-dimensional cells assuming small and moderate deformations from the circular shape. Their work will be discussed in more detail in §3 of this paper. The present computations for two-dimensional cells extend these solutions by accounting for transient motions and large deformations.

Another group of studies have considered three-dimensional flows, adopting various models for the cell membrane motion and mechanical properties. Keller & Skalak (1982) computed simple shear flow past an ellipsoidal cell of fixed shape. In their model, the tangential velocity of the membrane is prescribed so that the surface area of the membrane is conserved on a global but not on a local level. Sutera and coworkers used this model to illustrate streamline patterns and provide estimates for the membrane effective viscosity and elasticity (Sutera, Pierre & Zahalak 1989). The present model offers an improvement, in the sense that it allows both the cell shape and membrane tank-treading velocity to be computed as part of the solution. Richardson (1974, 1975) computed the deformation of oblate spheroidal capsules with linearly elastic interfaces during the initial stage of the motion. Brennen (1975) computed the effective viscosity of a suspension of spherical capsules for several types of interfacial behaviour. Barthès-Biesel and coworkers (Barthès-Biesel 1980; Barthès-Biesel & Rallison 1981; Barthès-Biesel & Sgaier 1985) studied the steady and transient deformation of mildly deformed capsules with elastic and viscoelastic interfaces. Pozrikidis (1994, 1995) computed the transient deformation of capsules bounded by viscous interfaces with constant surface tension or by elastic membranes. The present model for cells with incompressible interfaces is believed to reproduce the dynamics of red blood cell motion in a more accurate manner. For completeness, we also cite the numerical studies of Li, Barthès-Biesel & Helmy (1988) and Pozrikidis (1990) on the transient deformation of cells with elastic and incompressible membranes in uniaxial stagnation-point flow. Both of these studies were conducted using boundary integral methods.

In the present study we shall consider both two-dimensional and three-dimensional shapes. Studying the simplistic two-dimensional problem was found to be necessary in order to explore with adequate accuracy the behaviour at large deformations. Owing to constraints associated with high computational cost and numerical instabilities, studies of large three-dimensional deformations could not be carried out with satisfactory accuracy and are not reported. We find, however, that the two-dimensional and three-dimensional evolutions share a number of common features, and the former offers qualitative and in some cases quantitative information about the latter.

2. Problem statement and numerical method

We consider the deformation of a two-dimensional or three-dimensional capsule subject to a incident shear flow along the x-axis, $\boldsymbol{u}^{\infty} = (ky, 0, 0)$, where k is the shear rate.

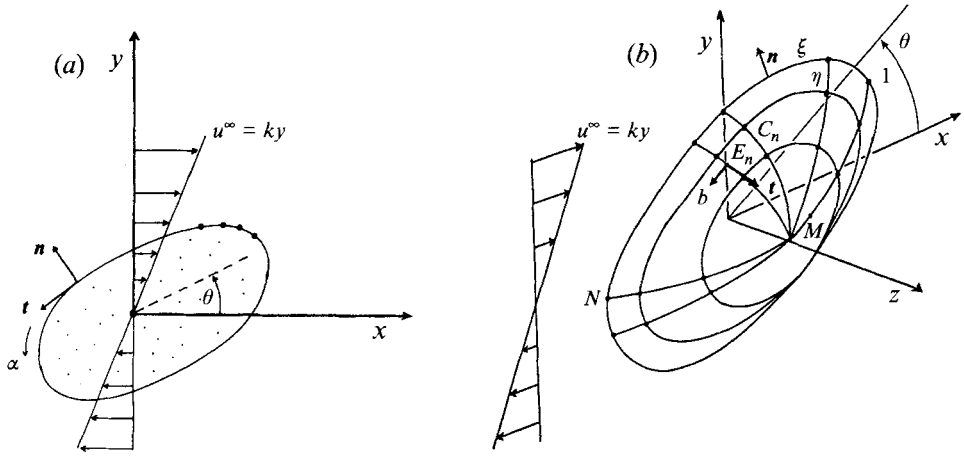

FIGURE 1. Schematic illustration of (*a*) a two-dimensional cell, (*b*) a three-dimensional cell placed in simple shear flow.

Schematic illustrations of instantaneous cell configurations are presented in figure 1(*a*, *b*). In the two-dimensional case we parametrize the membrane using a single variable α that takes values within the range $0 < \alpha < 2\pi$. For an elliptical cell, α is the natural polar coordinate of the elliptical coordinate system. In the three-dimensional case we introduce two curvilinear non-orthogonal surface coordinates ξ and η that take values within the ranges $0 < \xi < 2\pi$ and $-\pi/2 < \eta < \pi/2$. Discrete values of α and intersections of ξ- and η-lines yield interfacial grid points. It is consistent to regard the grid points either as Lagrangian point particles moving with the velocity of the fluid, or as plain interfacial markers moving with the velocity of the fluid normal to the interface.

Assuming that the flow occurs under conditions of creeping motion at vanishing Reynolds number, the velocity is continuous across the membrane of the cell, there is no slip between the lipid layers and the skeleton, and the viscosity of the cell is equal to that of the ambient fluid, we derive an integral representation for the velocity in terms of an interfacial distribution of point forces. In the case of three-dimensional flow we obtain

$$u_i(\boldsymbol{x}_0) = u_i^\infty(\boldsymbol{x}_0) - \frac{1}{8\pi\mu}\int_{Cell} G_{ij}(\boldsymbol{x}, \boldsymbol{x}_0)\,\Delta f_j(\boldsymbol{x})\,\mathrm{d}S(\boldsymbol{x}), \tag{1}$$

where $\boldsymbol{G}$ is the three-dimensional free-space Green's function or Stokeslet given by

$$G_{ij}(\boldsymbol{x}, \boldsymbol{x}_0) = \frac{\delta_{ij}}{\hat{\boldsymbol{x}}} + \frac{\hat{x}_i \hat{x}_j}{\hat{\boldsymbol{x}}^3}, \quad \hat{\boldsymbol{x}} \equiv \boldsymbol{x} - \boldsymbol{x}_0. \tag{2}$$

Details on the derivation of (1) may be found in standard texts on boundary integral methods (Pozrikidis 1992, chap. 5). For two-dimensional flow the differential surface element $\mathrm{d}S$ in (1) is replaced with the differential arclength $\mathrm{d}l$ and the coefficient 8π becomes 4π. The two-dimensional Stokeslet is given by

$$G_{ij}(\boldsymbol{x}, \boldsymbol{x}_0) = -\delta_{ij} \ln|\hat{\boldsymbol{x}}| + \frac{\hat{x}_i \hat{x}_j}{\hat{\boldsymbol{x}}^2}. \tag{3}$$

The density $\Delta \boldsymbol{f}$ of the Green's function distribution in (1) is equal to the discontinuity in the traction or surface force across the membrane. Assuming that the membrane is

a two-dimensional inviscid medium characterized by isotropic tension τ that acts in the plane of the interface, we write a force balance on a section of the membrane δM enclosed by the contour δC and obtain

$$\int_{\delta M} \Delta \boldsymbol{f} \, \mathrm{d}S = \int_{\delta C} \tau \boldsymbol{n} \times \boldsymbol{t} \, \mathrm{d}l, \tag{4}$$

where $\boldsymbol{n}$ is the normal vector pointing into the ambient fluid, and $\boldsymbol{t}$ is the tangent vector oriented in the counterclockwise sense with respect to $\boldsymbol{n}$ (Pozrikidis 1992, §5.5). Using the Stokes theorem and passing to the limit as the area of δM tends to zero, we obtain the differential force balance

$$\Delta \boldsymbol{f} = \tau 2\kappa_m \boldsymbol{n} - (\boldsymbol{I} - \boldsymbol{nn}) \cdot \nabla \tau, \tag{5}$$

where κ_m is the mean curvature of the interface, $\boldsymbol{I}$ is the identity matrix, and the projection operator $\boldsymbol{I} - \boldsymbol{nn}$ extracts the tangential component of a vector that it multiplies. The corresponding expression for two-dimensional flow is

$$\Delta \boldsymbol{f} = -\frac{\mathrm{d}(\tau \boldsymbol{t})}{\mathrm{d}l}. \tag{6}$$

Requiring that the membrane tension τ develops so that a differential element of the membrane deforms while maintaining its original surface area, we find that the instantaneous interfacial velocity field satisfies the kinematic condition

$$\boldsymbol{n} \cdot \left(\frac{\partial \boldsymbol{u}}{\partial \xi} \times \frac{\partial \boldsymbol{x}}{\partial \eta} + \frac{\partial \boldsymbol{x}}{\partial \xi} \times \frac{\partial \boldsymbol{u}}{\partial \eta} \right) = 0 \tag{7}$$

for three-dimensional flow, or

$$\boldsymbol{t} \cdot \frac{\partial \boldsymbol{u}}{\partial l} = 0 \tag{8}$$

for two-dimensional flow (Pozrikidis 1992, pp. 155, 168). Substituting (5) into (1) and then into (7) yields an integral equation of a non-standard type for the distribution of the tension over the cell surface, written in the symbolic form $F(\boldsymbol{x}; \tau) = 0$ where $\boldsymbol{x}$ represents a point on the membrane and the argument τ of F stands for the whole distribution of the tension over the interface. The problem is reduced to solving the integral equation, substituting the result back into (1), computing the velocity at the grid points, and then advancing the position of the grid points using either the total velocity of the fluid or the component of the velocity normal to the interface.

2.1. *Boundary element formulation*

To solve the integral equation $F(x; \tau) = 0$ we use a boundary element method that is similar to that developed previously by Pozrikidis (1993, 1994, 1995) to study the deformation of liquid drops with constant surface tension and viscous or elastic interfacial behaviour, but incorporates certain important new features.

In the case of three-dimensional flow, we discretize the surface of the cell into a set of N boundary elements $E_n, n = 1, \ldots N$, and then replace (1) with its discrete counterpart

$$u_i(\boldsymbol{x}_0) = u_i^{\infty}(\boldsymbol{x}_0) - \frac{1}{8\pi\mu} \sum_{n=1}^{N} S_n \langle G_{ij} \rangle_n \langle \Delta f_j \rangle_n, \tag{9}$$

where $\langle G_{ij}\rangle_n \equiv \frac{1}{S_n}\int_{E_n} G_{ij}(\boldsymbol{x},\boldsymbol{x}_0)\,\mathrm{d}S(\boldsymbol{x})$ and $\langle \Delta f_j\rangle_n \equiv \frac{1}{S_n}\int_{E_n} \Delta f_j(\boldsymbol{x})\,\mathrm{d}S(\boldsymbol{x})$ (10)

are the mean value of the Green's function and discontinuity in the surface force over the nth element, and S_n is the surface area of the nth element. The approximation in (9) is a variant of the trapezoidal rule. The corresponding discretization of the integral equation for two-dimensional flow follows by a straightforward change in notation.

The mean value of the jump in the traction in (10) may be computed by substituting (5) into the integrand and then applying numerical integration, but this requires the sensitive computation of the mean curvature and surface derivatives of the tension. To bypass these computations, we return to (4) and write

$$\langle \Delta \boldsymbol{f}\rangle_n = \frac{1}{S_n}\int_{C_n} \tau \boldsymbol{n}\times\boldsymbol{t}\,\mathrm{d}l(\boldsymbol{x}) \tag{11}$$

for three-dimensional flow, where C_n is the contour of the nth element and $\boldsymbol{t}$ is the tangential vector as shown in figure 1(*b*), or

$$\langle \Delta \boldsymbol{f}\rangle_n = \frac{1}{L_n}[(\tau\boldsymbol{t})_n - (\tau\boldsymbol{t})_{n+1}] \tag{12}$$

for two-dimensional flow, where L_n is the arclength of the nth element and $\boldsymbol{t}$ is the tangential vector pointing in the counterclockwise direction as shown in figure 1(*a*).

In the numerical method the contour integral in (11) is computed using the trapezoidal rule based on the values of the tension at the grid nodes. The integral equation $F(\boldsymbol{x};\tau) = 0$ for three-dimensional flow becomes

$$\boldsymbol{n}\cdot\left\{\frac{\partial \boldsymbol{u}^\infty}{\partial\xi}\times\frac{\partial\boldsymbol{x}}{\partial\eta}+\frac{\partial\boldsymbol{x}}{\partial\xi}\times\frac{\partial\boldsymbol{u}^\infty}{\partial\eta}-\frac{1}{8\pi\mu}\sum_{n=1}^{N} S_n\left[\left(\langle\Delta\boldsymbol{f}\rangle_n\cdot\frac{\partial\langle\boldsymbol{G}\rangle_n}{\partial\xi}\right)\times\frac{\partial\boldsymbol{x}}{\partial\eta}+\frac{\partial\boldsymbol{x}}{\partial\xi}\times\left(\langle\Delta\boldsymbol{f}\rangle_n\cdot\frac{\partial\langle\boldsymbol{G}\rangle_n}{\partial\eta}\right)\right]\right\} = 0. \tag{13}$$

For two-dimensional flow we obtain the corresponding form

$$\boldsymbol{t}\cdot\left(\frac{\partial\boldsymbol{u}^\infty}{\partial l}-\frac{1}{4\pi\mu}\sum_{n=1}^{N} S_n\langle\Delta\boldsymbol{f}\rangle_n\cdot\frac{\partial\langle\boldsymbol{G}\rangle_n}{\partial l}\right) = 0. \tag{14}$$

Both equations (13) and (14) may be written in the unified symbolic form

$$F(\boldsymbol{x};\tau_i,\boldsymbol{x}_i, i=1,\ldots,K) = 0, \tag{15}$$

where τ_i and $\boldsymbol{x}_i$ are the tension and position of the ith grid point, and K is the total number of boundary elements. The problem is reduced to solving (15) for the values of the tension at the grid nodes.

2.2. *Numerical solution of the integral equation*

A standard procedure for solving (15) is by point-wise collocation. This involves applying (15) at all grid points to derive a system of linear equations for the unknown tensions. Unfortunately, we found that this method leads to strong sawtooth-type numerical instabilities similar to those observed previously for axisymmetric flow (Pozrikidis 1990, §2.4). It is interesting to remark that these instabilities do not produce a corresponding conspicuous oscillation in the position of the marker points for two-

dimensional flow, but they do so in the case of three-dimensional flow. To control the instabilities in the case of two-dimensional flow, we applied the five-point smoothing formula of Longuet-Higgins & Cokelet (1976) with one or two consecutive passes. We found the best results are obtained if the position of the marker points is smoothed along with the distribution of the tension after each time step. A similar smoothing procedure for three-dimensional flow did not produce satisfactory results.

As an alternative to point-wise collocation with smoothing, we implemented a spectral projection method in which the membrane tension is expanded in a series of orthonormal basis functions. In the case of two-dimensional flow we expand the tension in a Fourier series with respect to arclength l as

$$\tau(l) = \alpha_0 + \sum_{n=0}^{N_F} [\alpha_n \cos(4\pi n l/L) + \beta_n \sin(4\pi n l/L)], \tag{16}$$

where L is the total arclength of the membrane and N_F is the total number of terms retained in the series. In the case of three-dimensional flow we use either the double Fourier expansion

$$\tau(\xi, \eta) = \sum_{m=0}^{M_F} \sum_{n=0}^{N_F} \cos(2m\eta)[\alpha_{mn} \cos(2\eta\xi) + \beta_{mn} \sin(2n\xi)] \tag{17}$$

or the Fourier–Legendre expansion

$$\tau(\xi, \eta) = \sum_{m=0}^{M_F} \sum_{n=0}^{N_F} P_m(2\eta)[\alpha_{mn} \cos(2n\xi) + \beta_{mn} \sin(2n\xi)], \tag{18}$$

where P_m is the mth-degree Legendre polynomial. Substituting (16), (17) or (18) into (15) and forming the projection of the resulting equation onto the basis functions we derive a system of linear equations for the coefficients α_n and β_n, or α_{mn} and β_{mn}. We have verified that (17) and (18) produce identical solutions for the membrane tension.

To illustrate the properties of the numerical method, in figure 2 we plot the instantaneous distribution of the membrane tension for an initially elliptical two-dimensional cell with aspect ratio $a/b = 8$, initial orientation angle $\theta_0 = 45°$, at time $kt = 4$ (see §3). The curves correspond to computations with the point-wise collocation method without smoothing, the point-wise collocation method with smoothing, the spectral method with $N_F = 4$, and the spectral method with $N_F = 8$. It is evident that the sawtooth instability is eliminated by applying smoothing. The curve generated using the spectral method with $N_F = 4$ lies close to that generated with $N_F = 8$ as well as to the curve generated by smoothing. Further experimentation showed that the spectral method is effective in removing the higher-order modes responsible for small-scale instabilities in agreement with previous experience (Krasny 1986), and the spectral method with $N_F = 8$ is capable of reproducing the distribution of the membrane tension with sufficient accuracy at least as long as the cell maintains a compact shape.

All computations of two-dimensional motions reported in §3 were conducted using the point-wise collocation method with smoothing, using 48 or 112 marker points over half of the cell membrane, and a time step of $k\Delta t = 0.05$. The integral of the Green's function $\boldsymbol{G}$ over each element of (8) is computed using the four-point Gauss quadrature after the singularity is subtracted off from the integrand, and the cell contour is approximated using cubic splines with respect to the parameter α. The membrane is considered to have reached a steady state when the orientation angle, computed in

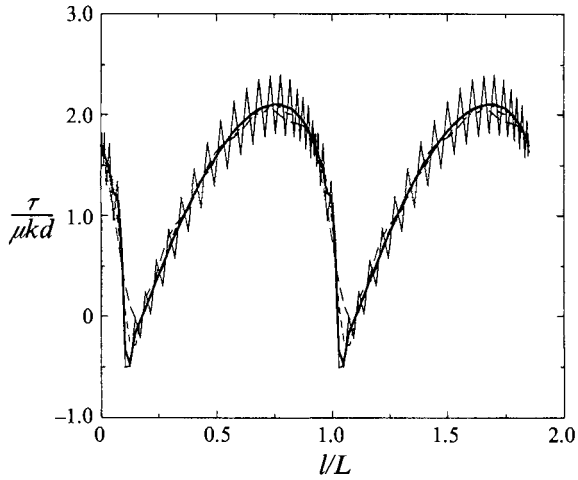

FIGURE 2. Comparison of the distributions of the membrane tension around an initially two-dimensional elliptical cell with aspect ratio $a/b = 8$, initial orientation angle $\theta_0 = 45°$ at time $kt = 4$ computed suing: (*a*) the primary point-wise collocation method (solid line); (*b*) the point-wise collocation method with the five-point smoothing formula (bold solid line); (*c*) the spectral method with $N_F = 4$ (long-dashed line); and (*d*) the spectral method with $N_F = 8$ (dashed line).

terms of the eigenvectors of the inertial tensor of the cell body, and the Taylor deformation parameter, defined as $D = (L-B)/(L+B)$ where L and B are the maximum and minimum dimension of the cell respectively, have reached well-defined plateaus. The area of the cell is renormalized at every time step, and the maximum change in the membrane arclength due to numerical error for a cell that is initially aligned with the x-axis is less than 3% the initial value. For cells with initial inclination angle of $\pi/4$, the maximum change in the membrane arclength is less than 0.1% of the initial value.

The computations for three-dimensional cells presented in §4 were conducted using the spectral expansion (14) with $M_F = 4$ and $N_F = 4$, using 16 collocation points in the ξ-direction and 8 collocation points in the η-direction which results in a total of 108 boundary elements over a quarter of the cell membrane, and a time step of $k\Delta t = 0.05$. The surface coordinate lines are approximated using cubic splines with respect to ξ or η. The computation of the integrals of the Green's function over the interfacial elements is discussed by Pozrikidis (1995). Steady state is considered to have been reached when the cell orientation angle and the Taylor deformation parameter computed from the membrane contour in the (x, y)-plane have reached well-defined asymptotic values. The cell volume is renormalized at each time step, and the maximum change in the membrane surface area is less than 1.5% the initial value.

All computations were performed on SPARCstation 1 SUN computers. Each complete run required approximately 6 h or 30 h respectively for two-dimensional or three-dimensional flow.

2.3. *Effective stresses and membrane tank-treading frequency*

In the case of two-dimensional flow we compute the effective stress tensor of a dilute suspension of cells in shear flow using the equation

$$\langle \sigma_{ij} \rangle = -\delta_{ij}\langle P \rangle + 2\mu \langle e_{ij} \rangle + \Phi \int_{Cell} \tau t_i t_j \, \mathrm{d}l, \tag{19}$$

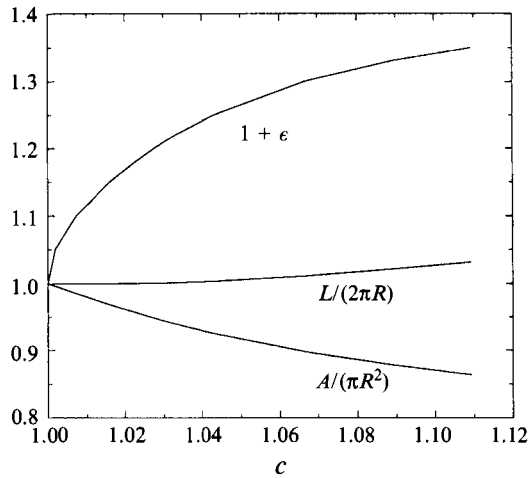

FIGURE 3. Characteristics of a family of two-dimensional stationary deformed cells enclosed by incompressible membranes (Zahalak *et al.* 1987). The dimensionless shear rate ϵ, cell area $A/\pi R^2$ and perimeter $L/2\pi R$ as functions of the circularity c; R is the mean cell radius.

where $\langle\ \rangle$ denotes the areal average, P is the pressure, e_{ij} is the rate-of-strain tensor, and Φ is the number of cells per unit area of the suspension (Zhou & Pozrikidis 1993*b*). In the case of three-dimensional flow we use the analogous form

$$\langle\sigma_{ij}\rangle = -\delta_{ij}\langle P\rangle + 2\mu\langle e_{ij}\rangle + \Phi\int_{Cell}\tau(\delta_{ij}-n_i n_j)\,\mathrm{d}S, \tag{20}$$

where $\langle\ \rangle$ denotes the volume average and Φ is the number of cells per unit volume.

Under the action of the shear flow, the cell membrane will engage in a tank-treading motion around the cell interior. For two-dimensional flow, we define the tank-treading frequency f and period T as

$$f = \frac{2\pi}{T}, \quad T = \int_{Cell}\frac{\mathrm{d}l}{u_t}, \tag{21}$$

where u_t is the tangential component of the membrane velocity called the tank-treading velocity. At steady state u_t is constant around the cell contour. For three-dimensional flow, we calculate T using (21) with the tangential velocity computed around the trace of the membrane in the (x, y)-plane.

3. Two-dimensional cells

We consider the transient deformation of a two-dimensional cell subject to a simple shear flow as shown in figure 1(*a*). We non-dimensionalize all variables using as characteristic length the equivalent radius $d = (A/\pi)^{1/2}$ where A is the cross-sectional area of the cell, velocity kd, time $1/k$, stress μk, and tension μkd, and find that the motion depends upon the initial cell configuration alone; no physical constants enter the statement of the problem. When the cell has an elliptical shape in the undeformed state, the motion may be considered a function of the aspect ratio a/b or reduced membrane perimeter length $c = L/(2\pi d)$ defined here as the cell circularity, as well as initial inclination angle θ_0.

3.1. *A family of steady deformed cells*

Zahalak *et al.* (1987) computed a family of stationary cells with incompressible interfaces suspended in a simple shear flow. The shapes of the cells are parametrized by the reduced shear rate ϵ which is analogous to the capillary number, and ratio of the viscosities of the cell and suspending fluid λ. Their asymptotic analysis requires that the cells exhibit small deviations from the circular shape corresponding to $\epsilon = 0$. In addition to computing steady shapes, Zahalak *et al.*, provided illustrations of the streamline patterns and distributions of membrane tension and external and internal interfacial tractions.

To compare the results of our numerical computations to those of the asymptotic analysis, we note that to every value of ϵ there corresponds a value of the circularity c. The relation between these two parameters may be found using the equations for the cell shape provided by Zahalak *et al.* In figure 3 we plot ϵ, reduced cell area $A/(\pi R^2)$, and reduced perimeter $L/(2\pi R)$ as functions of c, where R is the mean cell radius defined as

$$R = \frac{1}{2\pi}\int_0^{2\pi} r \, \mathrm{d}\theta \tag{22}$$

and r is the radial distance from the origin around the cell. The curves end at $c = 1.1092$ or $\epsilon = 0.35$, which is close to the point where the asymptotic analysis ceases to be valid.

3.2. *Evolution of elliptical cells*

Our computations show that an initially elliptical cell with $c = 1.0301$ or $a/b = 1.5$ deforms and reaches a stationary shape in which the membrane engages in a tank-treading motion around the cell with uniform tangential velocity. In figure 4(*a*) we present three superposed steady membrane profiles corresponding to three different initial inclination angles θ_0. The corresponding initial cell profiles are shown on the right column. We find that for all three inclinations, the cell deforms into the same steady asymptotic shape, and this suggests the existence of a unique steady state. At this relatively small value of $c-1$ the differences between the initial elliptical shape and the asymptotic shape are small, and deviations in aspect ratio are masked by numerical error. The open circles in figure 4(*a*) show the steady-state profile predicted by the perturbation analysis of Zahalak *et al.* corresponding to $\epsilon = 0.1793$. We find good agreement between the asymptotic predictions and the numerical computations, and this serves to validate the numerical method.

The distribution of the membrane tension τ and tank-treading velocity u_t at steady state are plotted in figure 5(*a*) in radial format. We note that u_t is uniform around the perimeter of the cell, as required by the condition of membrane incompressibility, but the distribution of the tension shows a noticeable nearly sinusoidal variation which is out of phase with the membrane curvature; the points of maximum and minimum tension are located near the points of minimum and maximum curvature. The agreement among the three computations for different initial inclination angles on the steady state tank-treading velocity is excellent, but we observe noticeable differences in the membrane tension. The latter is evidence of the fact that a small change in membrane shape results in relatively large changes in membrane tension around a cell with small aspect ratio. Further information on the magnitude of u_t and τ will be presented later in figure 6. The open circles in figure 5(*a*) show the asymptotic values of τ and u_t computed using equations (60) and (54) of Zahalak *et al.* (1987). The asymptotic value of τ is closer to the numerical values for $\theta_0 = 0$ and 90°, than for $\theta_0 = 45°$, but this is a rather fortuitous coincidence.

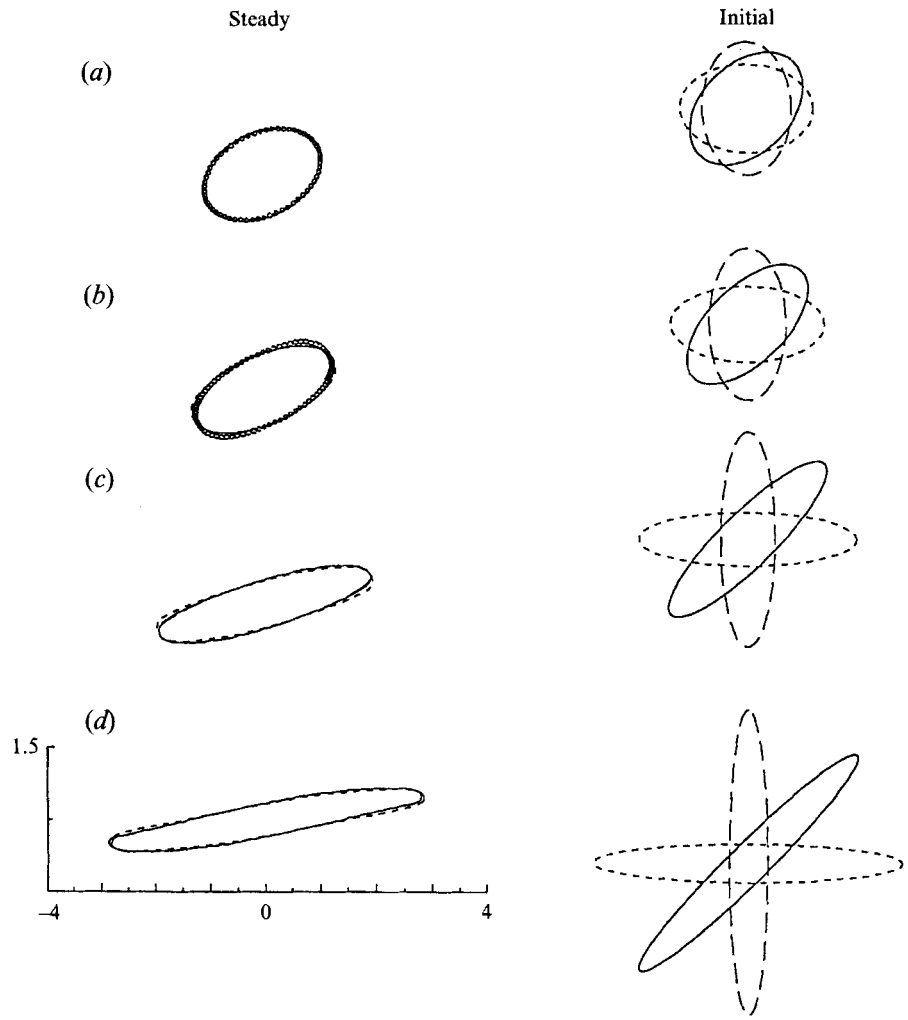

FIGURE 4. Steady shapes of two-dimensional cells corresponding to (*a*) $a/b = 1.5$ or $c = 1.0301$; (*b*) $a/b = 2$ or $c = 1.0896$; (*c*) $a/b = 4$ or $c = 1.3648$; and (*d*) $a/b = 8$ or $c = 1.8422$. The dashed lines are for $\theta_0 = 0°$, the solid lines for $\theta_0 = 45°$, the long-dashed lines for $\theta_0 = 90°$. The corresponding initial cell profiles are shown next to the steady shapes. The open circles represent the asymptotic solution of Zahalak *et al.* (1987).

Computations with moderate values of circularity showed similar behaviours. For instance, when the circularity is increased to 1.0896 corresponding to $a/b = 2$, the deformation leads to a steady-state profile that is independent of θ_0, as shown in figure 4(*b*). In this case, the asymptotic analysis of Zahalak *et al.* (1987) overestimates the magnitude of the cell orientation at steady state. This is not surprising, for $c = 1.0896$ corresponds to the maximum shear rate at which the asymptotic analysis is expected to be valid. Further computations showed that a cell with high circularity deforms in a smooth manner and attains a steady shape that is significantly different from the initial elliptical shape. Figure 4(*c*, *d*) illustrates steady cell profiles along with the initial cell shapes for $a/b = 4$ and 8, corresponding to $c = 1.3648$ and 1.8422. In both cases the steady shape was found to be insensitive to the initial cell inclination angle θ_0, suggesting the existence of a unique steady state.

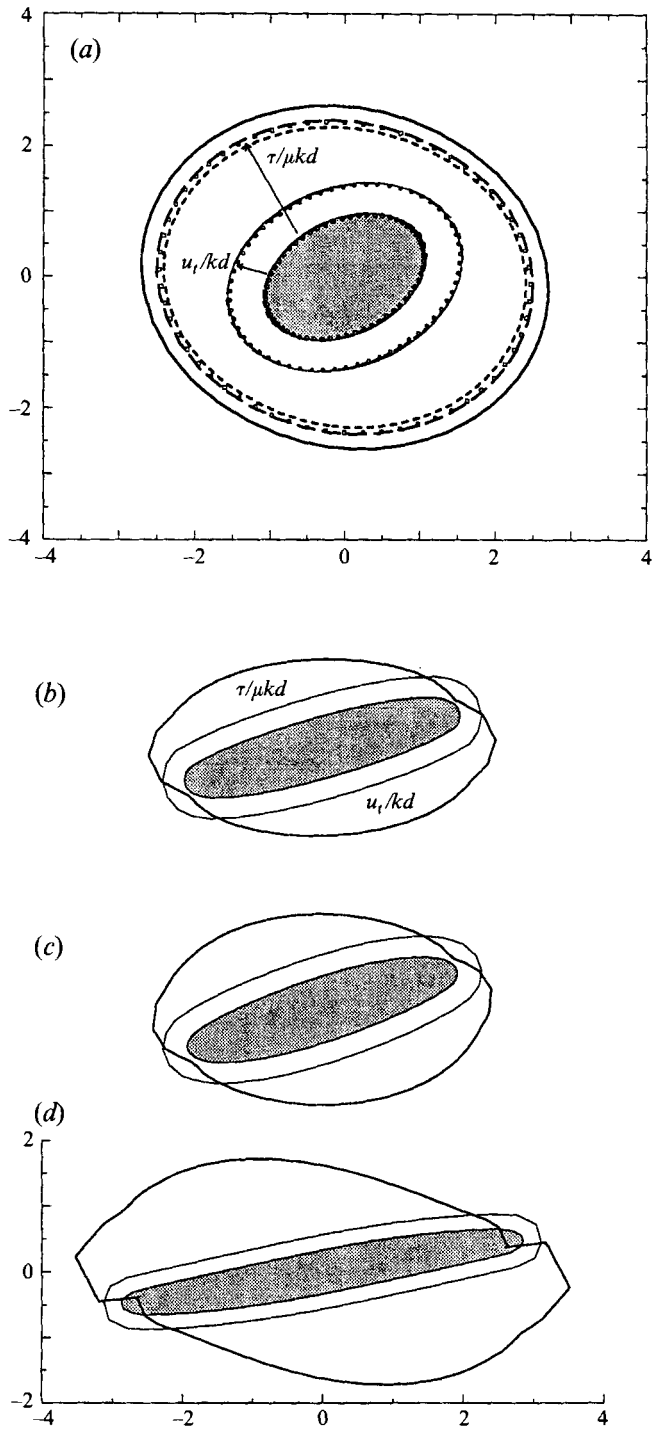

FIGURE 5. The distributions of membrane tension and tank-treading velocity plotted in a radial format. The value of the tension or tank-treading velocity corresponding to a particular point is proportional to the length of the line segment that is perpendicular to the membrane and extends up to the corresponding contours as shown in panel (*a*). The dashed line is for $\theta_0 = 0°$, the solid line for $\theta_0 = 45°$, the long-dashed line for $\theta_0 = 90°$. Open circles represent the asymptotic solution of Zahalak *et al.* (1987). (*a*) $a/b = 1.5$, (*b*) $a/b = 4$, $\theta_0 = 0°$; (*c*) $a/b = 4$, $\theta_0 = 45°$; (*d*) $a/b = 8$, $\theta_0 = 0°$.

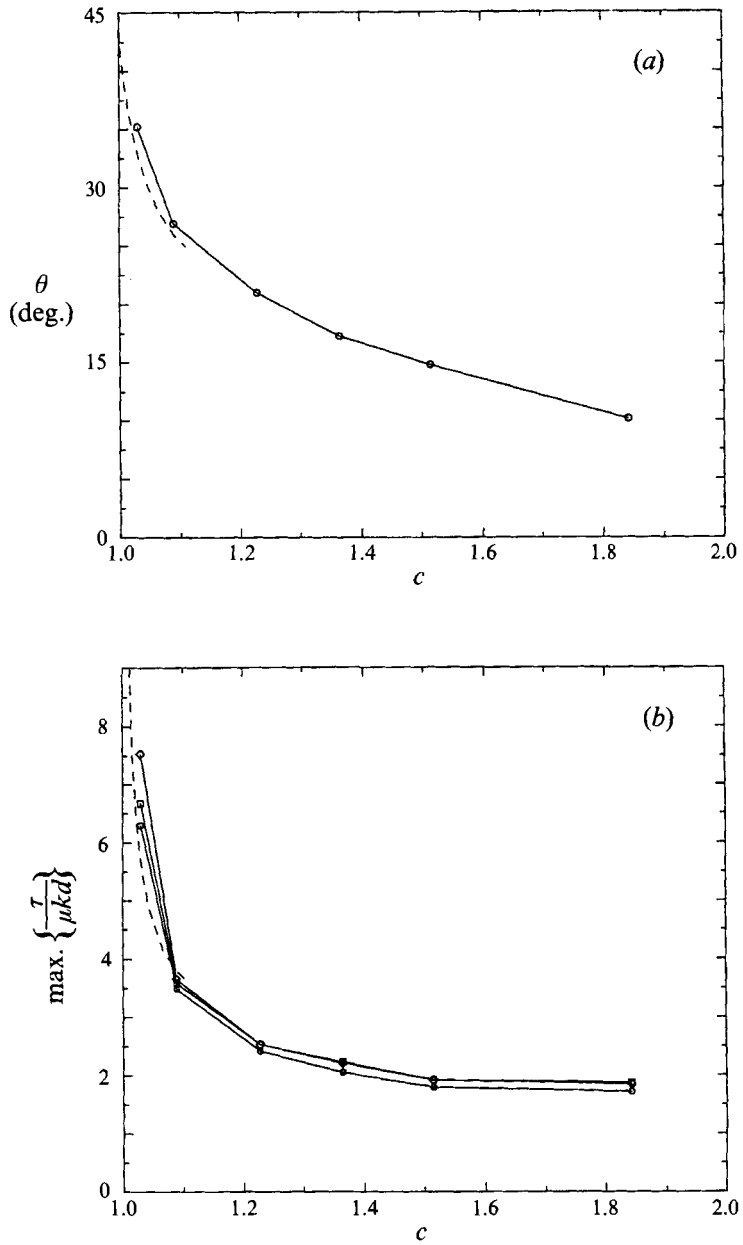

FIGURE 6(*a*,*b*). For caption see facing page.

The distributions of membrane tension and tank-treading velocity corresponding to the highly deformed cells are shown in figure 5(*b*, *c*, *d*). The tank-treading velocities are constant around the membrane, but the tensions show significant variations with higher values along the flattened upper and lower side of the cells. In the case $a/b = 4$ the tension is positive all around the cell, which indicates that the membrane is being stretched, whereas for $a/b = 8$ the tension is positive over the major portion of the membrane and becomes negative near the tip where the membrane curvature is highest, which indicates that the membrane is locally compressed. A truly incompressible

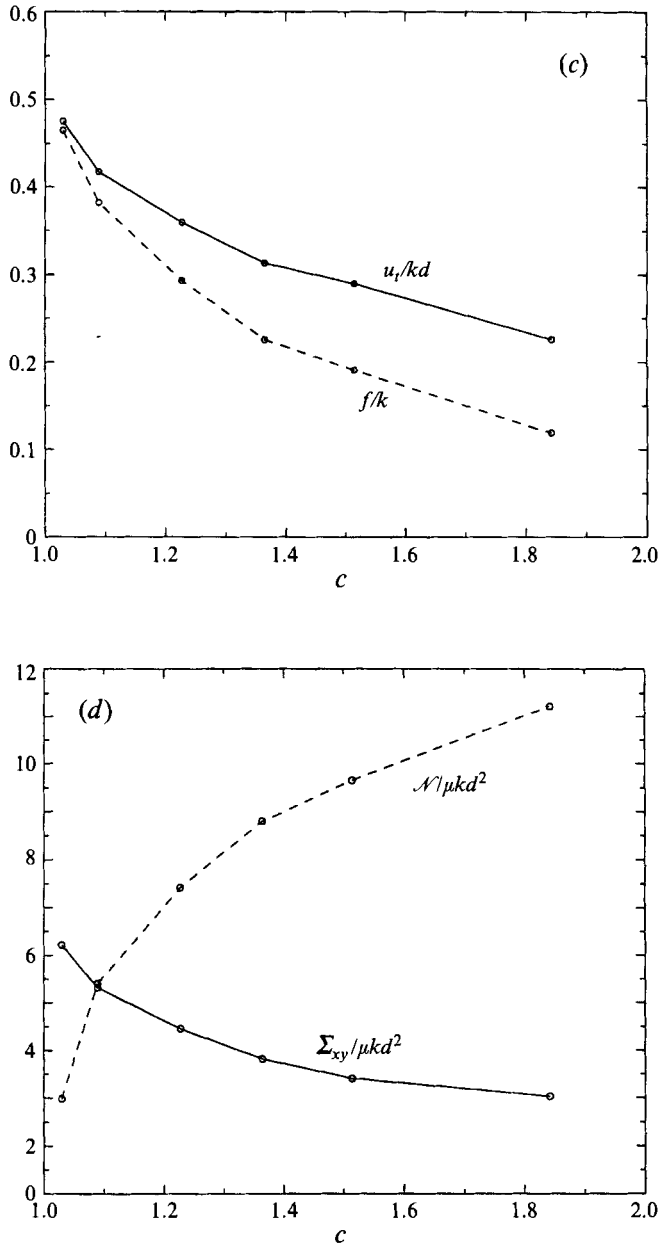

FIGURE 6. (*a*) The orientation angle of a two-dimensional cell at steady state as a function of circularity c. Open circles show the computed values, and the dashed line represents the predictions of the asymptotic analysis of Zahalak *et al.* (1987). (*b*) The maximum tension τ_{max} as a function of c. Open circles represent the computed values corresponding to $\theta_0 = 0°$, open diamonds to $\theta_0 = 45°$, open squares to $\theta_0 = 90°$, and the dashed line corresponds to the asymptotic analysis of Zahalak *et al.* (*c*) The computed tank-treading velocity (solid line) and frequency (dashed line) as functions of c. (*d*) The effective shear stress (solid line) and normal stress difference (dashed line).

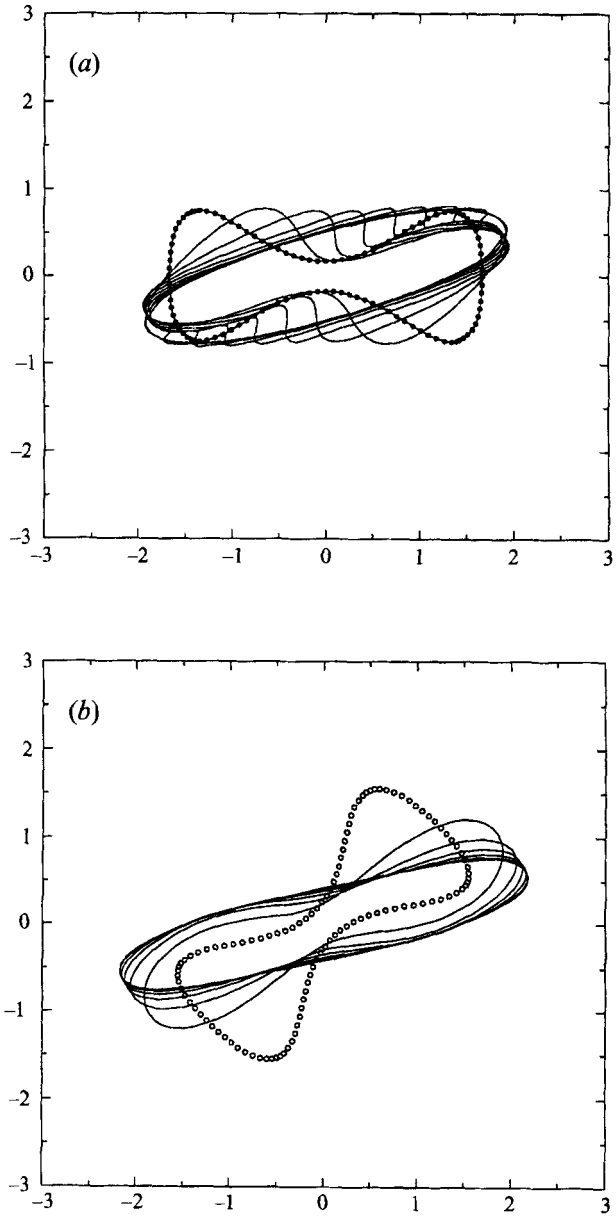

FIGURE 7(*a*,*b*). For caption see facing page.

membrane will develop wrinkles at that point, but numerical smoothing emulates bending elasticity and prevents the occurrence of small-scale oscillations.

3.3. *Steady shapes*

The numerical computations suggest that the steady shape of an initially elliptical cell is a single-valued function of the circularity. In turn, this suggests that the geometrical and dynamic properties of steadily deformed two-dimensional cells may be described in terms of the aspect ratio a/b or circularity c. In figure 6(*a*) we plot the steady orientation angle θ as a function of c, and find that nearly circular cells are oriented

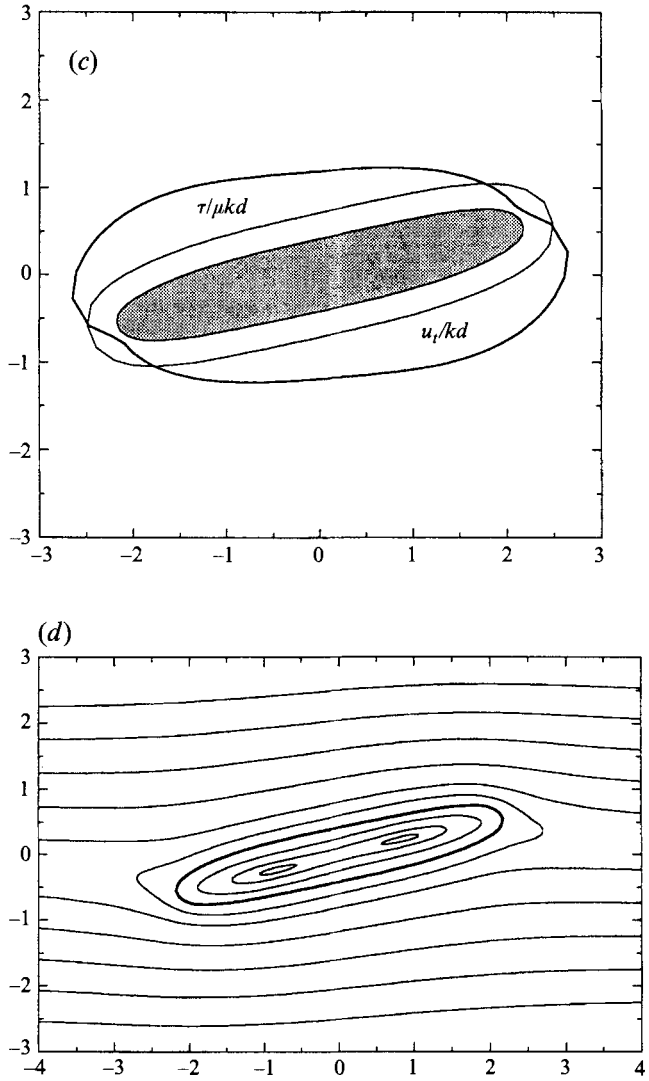

FIGURE 7. (*a*) A sequence of evolving profiles of an initially biconcave cell aligned with the shear flow at $kt = 0, 1, 2, \ldots, 9$. (*b*) A sequence of evolving profiles for $\theta_0 = 45°$ at $kt = 0, 1, 2, \ldots, 6$. The initial shapes are shown with open circles. (*c*) The corresponding distribution of membrane tension (bold solid line) and tank-treading velocity (solid line) around the membrane at steady state in radial format. (*d*) The streamline pattern inside and outside the cell at steady state.

along the major principal axis of rate of strain of the shear flow, at an angle of 45°, whereas highly elongated cells tend to align with the flow. The dashed curve in figure 6(*a*) represents the asymptotic predictions of Zahalak *et al.* (1987) which are seen to provide a natural extension of the numerical data towards small values of c.

The maximum membrane tension τ_{max} is an important variable for the study of membrane failure and cell hemolysis. Experiments have shown that when τ_{max} exceeds a threshold which is somewhere between 5 and 10 dyn cm^{-1} depending upon physiological conditions, the membrane is likely to fail. In figure 6(*b*) we plot τ_{max} as a function of c for three different values of θ_0, and obtain small variations around well-defined mean values. In the limit as c tends to one, τ_{max} becomes singular, which

indicates that an infinite tension is required to resist the shearing deformation and maintain the circular shape. As c is increased, τ_{max} is reduced, and as c tends to infinity, in which case the cell resembles a thin sheet, τ_{max} reaches an asymptotic value that is roughly equal to $1.75\mu kd$. The dashed curve in figure 6(*b*) represents the asymptotic solution obtained using equation (59) of Zahalak *et al.* For small values of c, the computed values of τ_{max} are in good agreement with the asymptotic predictions.

In figure 6(*c*) we plot the tank-treading velocity u_t and tank-treading frequency f at steady state as functions of c, and find that both are reduced as c is increased. The computed values of u_t are in good agreement with the asymptotic predictions of Zahalak *et al.* at small values of c.

One motivation for studying the behaviour of the individual blood cells is to investigate the rheological properties of blood. In figure 6(*d*) we plot the effective shear stress Σ_{xy} and normal stress difference $\mathcal{N} = \Sigma_{xx} - \Sigma_{yy}$ of a dilute suspension, where Σ is the last term on the right-hand side of (19). For a circular cell Σ_{xy} has a finite value whereas $\mathcal{N}$ is equal to zero due to the spatial isotropy of the cell shape. As c is increased, the effective shear stress decreases because the cell becomes more elongated and tends to align with the shear flow, therefore effectively reducing the rate of viscous dissipation within the flow. The normal stress difference increases as a result of anisotropy attributed to the increasingly elongated cell shape.

3.4. *Deformation of cells with biconcave shapes*

The above discussion was based on numerical computations for cells with elliptical initial shapes. To examine whether a cell with a convoluted shape might deform in a significantly different way and obtain a different asymptotic shape, as well as to assess the effectiveness of the numerical method for more complex cell geometries, we consider the deformation of cells whose undeformed shape resembles the mid-plane cross-sectional shape of a normal red blood cell as described by Evans & Fung (1972). The initial cell shape is described by a properly scaled version of the equation

$$y' = 0.5(1-x'^2)^{1/2}(c_0 + c_1 x'^2 + c_2 x'^4), \tag{23}$$

where $-1 < x' < 1$, $c_0 = 0.207161$, $c_1 = 2.002558$, $c_2 = -1.122762$, and the x'- and y'-axes are oriented along the cell's major and minor axis. The corresponding circularity is $c = 1.515$.

In figure 7(*a*, *b*) we present sequences of evolving cell profiles for two initial orientations. When the cell is initially aligned in the direction of the flow, the deformation leads to formation of two symmetric pockets originating at the dimples as shown in figure 7(*a*). As the cell deforms, the depth of the pockets is reduced and the cell attains a smooth, nearly elliptical steady shape. When the cell is initially aligned at 45° with respect to the x-axis, it stretches under the action of the shear flow and obtains the same nearly elliptical steady shape without developing any pockets or dimples as shown in figure 7(*b*).

Comparing the steady shapes shown in figures 7(*a*) and 7(*b*) with each other as well as to the steady shape corresponding to an initially elliptical cell with identical circularity, we find only minor differences attributed to numerical error. This observation confirms that for a cell of a given circularity, the stationary shape in shear flow is independent of the initial shape as long as this is not significantly convoluted so that the cell may fold during the deformation. The transient motion and time it takes for the cell to reach the stationary shape, however, show strong dependences on the initial configuration. For instance, the times at which the biconcave cells shown in figures 7(*a*) and 7(*b*) reach stationary shapes are approximately $kt = 9$ and 6.

The distribution of membrane tension and membrane tank-treading velocity at steady state corresponding to evolutions shown in figure 7(*a*, *b*) are illustrated in figure 7(*c*). As in the case of elliptical cells, we observe that the tension is minimum near the point of maximum membrane curvature and vice versa, whereas u_t is uniform along the membrane. The values of τ_{max} and u_t may be read off figure 6(*b*, *c*) for $c = 1.515$. Experimental observations have shown that the membrane is likely to fail when τ_{max} exceeds a critical value that is between 5 and 10 dyn cm^{-1}. Using the maximum value we derive a limit on the maximum shear stress under which the cells will remain intact, $\sigma_{max} = \frac{1}{2}$ (10 dyn cm^{-1})/(5 μm) = 1000 dyn cm^{-2}, where we have used the value $d =$ 5 μm for the equivalent cell radius. This estimate is in good agreement with the experimental observations of Sutera & Mehradi (1975) and Beissinger & Laugel (1978).

Experiments have shown that the tank-treading frequency f of human erythrocytes suspended in a medium of comparable viscosity is a nearly linear function of shear rate and varies considerably with cell age. When normalized by the shear rate, f/k is roughly equal to 0.22 for young cells and 0.18 for older cells (Tran-Son-Tay, Sutera & Rao 1984). The computed value of f/k corresponding to figure 7(*c*) is 0.19, which is remarkably close to that of real three-dimensional red blood cells. This successful comparison suggests that the evolution of the two-dimensional cells reveals some salient features of the natural three-dimensional motion. Caution, however, should be exercised in applying these results to red blood cells in view of the strong assumptions regarding the cell membrane mechanical properties.

To gain further insights into the structure of the flow inside and outside the cell, in figure 7(*d*) we present a streamline pattern at steady state. Zahalak *et al.* (1987) found that the streamlines inside cells with small aspect ratio form a single eddy. We find two small internal eddies enclosed by a larger eddy lining the membrane. A similar double-eddy pattern has also been observed inside liquid drops whose viscosity is significantly lower than that of the suspending fluid (Kennedy, Pozrikidis & Skalak 1994), but has not been reported in previous studies on blood cell flow. The occurrence of two eddies inside the cell is attributable to the highly elongated cell shape. The general features of the streamline pattern outside the cell are similar to those found by Zahalak *et al.* for mildly deformed cells, as well as those occurring around sheared two-dimensional drops (Zhou & Pozrikidis 1993*a*). In all cases, the external flow includes a region of recirculating flow enclosed by a closed dividing streamline.

4. Three-dimensional cells

We consider next the deformation of the three-dimensional cell illustrated in figure 1(*b*). Non-dimensionalizing all variables as discussed in §3 using as characteristic length the equivalent cell radius $d = (3V/4\pi)^{1/3}$ where V is the cell volume, we find that the motion depends only upon the initial cell shape. For a cell with an oblate spheroidal initial shape with major and minor axes equal to a and b, the motion is a function of the aspect ratio a/b or sphericity $s = S/(4\pi d^2)$ where S is the surface area, and initial inclination angle θ_0.

To describe the shape of the membrane we introduce a system of two curvilinear non-orthogonal surface coordinates ξ and η as discussed in §2. Initially, the ξ-lines are parallel to the (x, y)-plane, and the η-lines lie in planes that pass through the z-axis, as shown in figure 8(*a*). In the most accurate computations we discretize the membrane using 32 divisions in both the ξ- and η-directions. Owing to the dual symmetry of the cell shape, it suffices to compute the deformation of the upper front quarter of the cell alone, which is described by a 16×8 grid of marker points. To avoid severe grid

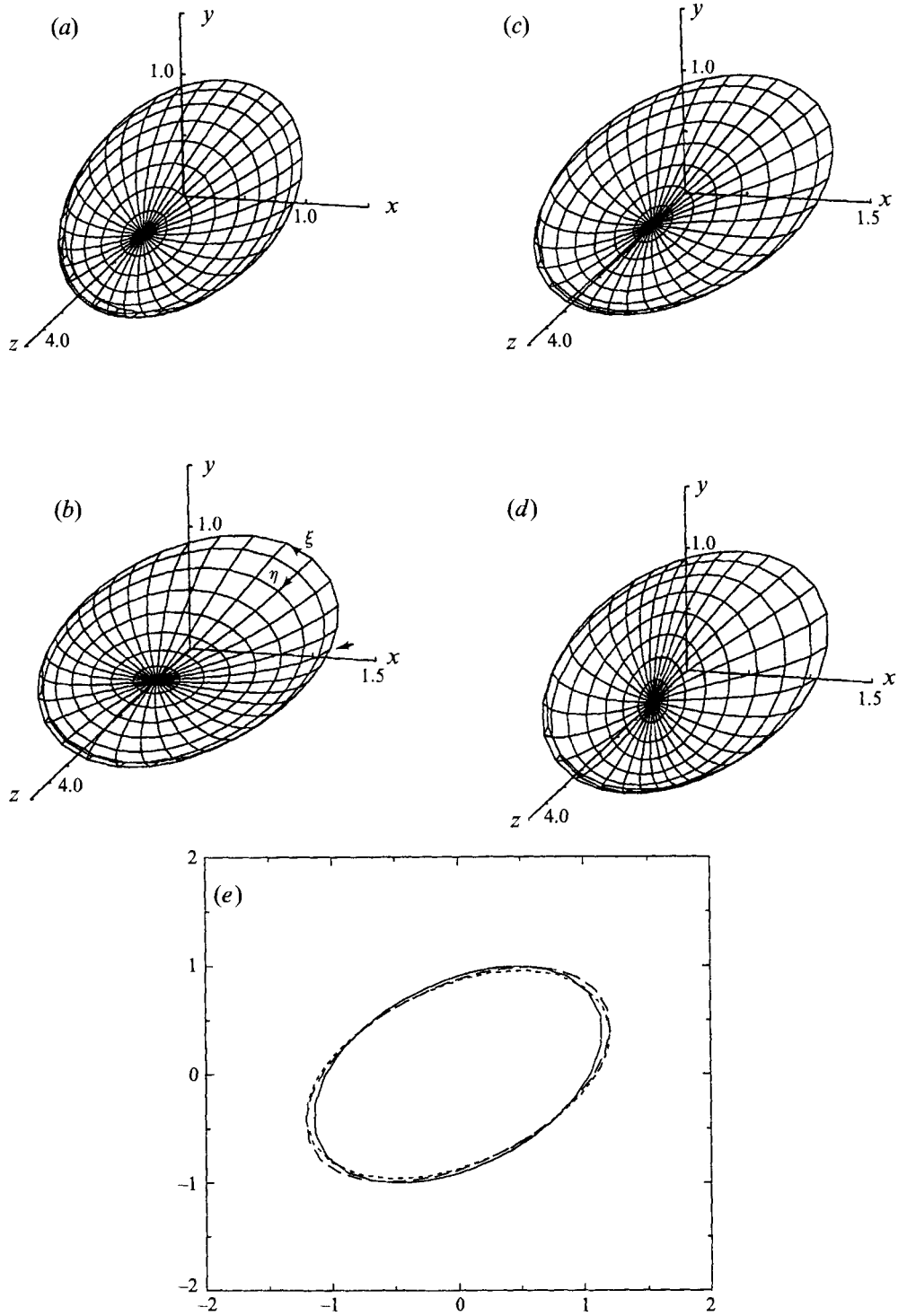

FIGURE 8. (*a*) The surface grid on an oblate spheroidal cell with $a/b = 1.5$ and $\theta_0 = 45°$ at the initial instance. The shape of half the cell near steady state for (*b*) $\theta_0 = 0°$, (*c*) $\theta_0 = 45°$, and (*d*) $\theta_0 = 90°$, and (*e*) their projection in the (x, y)-plane. The dashed line is for $\theta_0 = 0°$, the solid line for $\theta_0 = 45°$, the long-dashed line for $\theta_0 = 90°$.

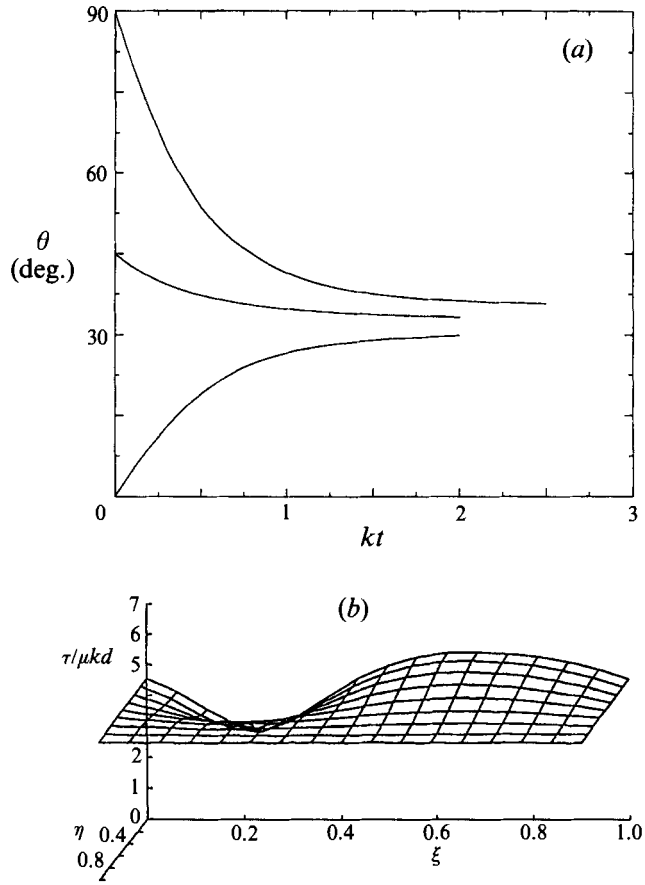

FIGURE 9. (*a*) The evolution of the cell orientation angle for $a/b = 1.5$. (*b*) The membrane tension distribution as a function of the surface coordinates ξ and η for $a/b = 1.5$, $\theta_0 = 0°$ at steady state. The $\xi = 0$ line is indicated in figure 8(*b*) with an arrow.

deformations and concomitant numerical inaccuracies, we advance the position of the marker points using the normal component of the membrane velocity.

In figure 8(*a*) we show the initial shape of a cell with aspect ratio $a/b = 1.5$ corresponding to $s = 1.031$, oriented at $\theta_0 = 45°$. Under the action of the external shearing forces the cell deforms from the initially ellipsoidal shape to a steady state shown in figure 8(*c*) in which the cell membrane tank-treads steadily around the interior fluid. The tank-treading velocity is a function of location over the membrane as required by the condition of incompressibility. In figure 8(*b*, *c*, *d*) we show half of the cell surface at steady state corresponding to three initial inclinations $\theta_0 = 0°$, 45°, 90°, and in figure 8(*e*) we plot the projections of the steady shapes on the (x, y)-plane. Attributing the small differences to numerical error suggests that the steady shape is independent of the initial orientation. The evolution of the cell inclination angle is shown in figure 9(*a*), where we observe that all three curves tend to the asymptotic value 33°.

In figure 9(*b*) we present the distribution of the membrane tension at steady state corresponding to $\theta_0 = 0°$. To make a correspondence between the physical location of points on the membrane and the location in the surface coordinate plane, in figure 8(*b*) we have indicated the η-line corresponding to $\xi = 0$ with an arrow. Inspecting figure

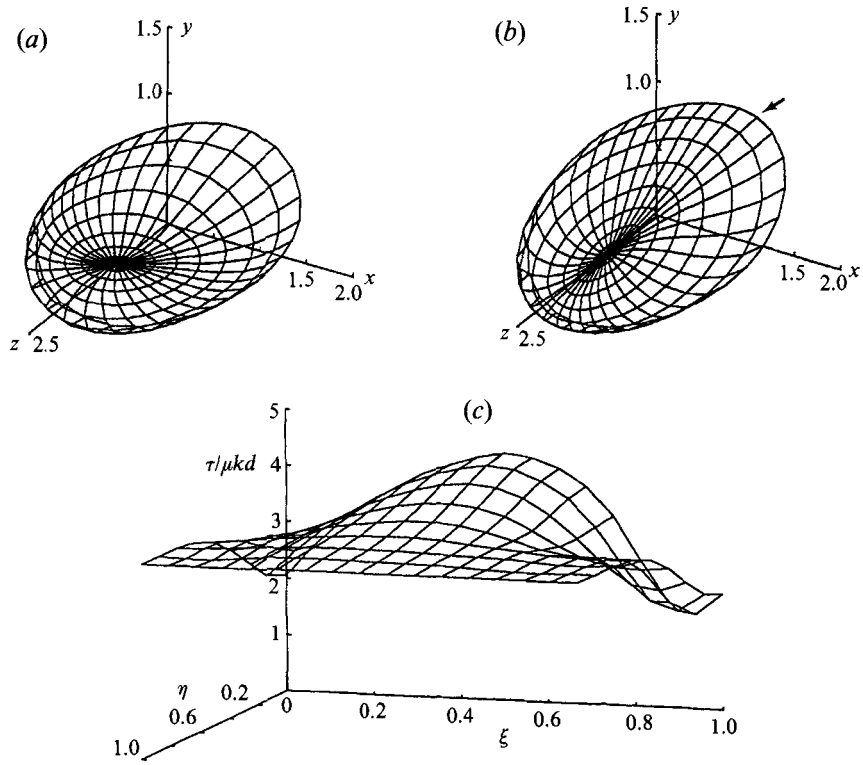

FIGURE 10. The shape of half the cell at steady state for $a/b = 2$ and (a) $\theta_0 = 0°$, (b) $\theta_0 = 45°$. (c) The membrane tension distribution as a function of ξ and η for $\theta_0 = 45°$. The $\xi = 0$ line is indicated in figure 10(b) with an arrow.

9(b) in conjunction with figure 8(b) shows that τ is inversely proportional to the membrane curvature, and reaches a maximum at some point in the (x, y)-plane on the upper surface towards the rear end of the cell. This feature is familiar from the case of two-dimensional flow.

Steady cell shapes for a larger aspect ratio $a/b = 2$, corresponding to $s = 1.095$ are shown in figure 10(a, b) for $\theta_0 = 0°$ and 45°. The fact that these two shapes are almost identical with small differences attributed to numerical error suggests that the asymptotic steady shape is unique. A plot of the corresponding membrane tension distribution for $\theta_0 = 45°$, shown in figure 10(c), reveals that τ reaches a maximum near the point of minimum membrane curvature.

To illustrate the three-dimensional nature of the computed steady cell shapes from a different perspective, in figure 11(a, b) we show the projection of cells onto the (x, y)-plane which is perpendicular to the direction of the mean velocity gradient, for $a/b = 1.5$, 2 or $s = 1.031$, 1.095, corresponding to the initial angle $\theta_0 = 45°$. This is the perspective captured by photographs of red blood cells through a cone-and-plate viscometer (rheoscope). The sphericity s of normal red blood cells is equal to 1.256 for old cells and 1.262 for young cells. These values are significantly higher than the ones described above for $a/b = 1.5$ and 2. Unfortunately, because of numerical instabilities, computations for cells with higher aspect ratios could not be carried out with sufficient accuracy.

In figure 11(c) we present a sequence of photographs of normal red blood cells suspended in a dextran-saline solution at successive time intervals, taken from Fischer

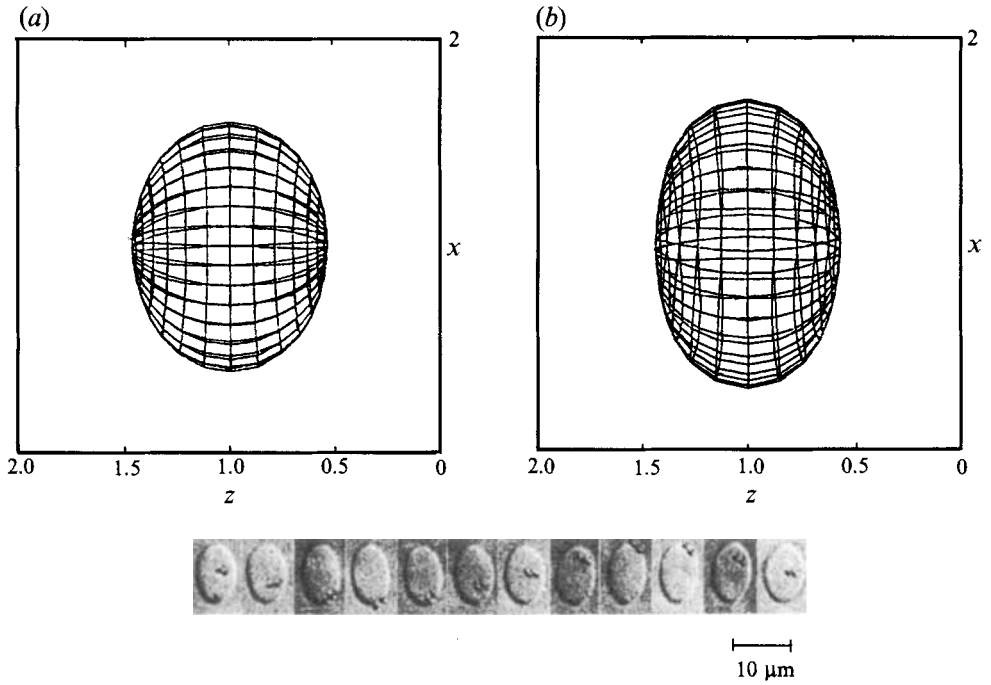

FIGURE 11. Projections of the steady cell shape onto the (x, z)-plane for (*a*) $a/b = 1.5$ and $\theta_0 = 45°$; (*b*) $a/b = 2$ and $\theta_0 = 45°$. (*c*) A sequence of photographs of red blood cells suspended in dextran-saline solution during viscometric flow in a cone-and-plate chamber at $k = 46\ \text{s}^{-1}$ (Fischer *et al.* 1978). The photographs are taken at time interval of 83 ms.

s	A_{xy}	A^a_{xz}	θ	$\tau_{max}/\mu kd$	f/k	$\Sigma_{xy}/\mu k$	$\mathcal{N}_1/\mu k$	$\mathcal{N}_2/\mu k$
1.031	0.26	1.30	33.2	5.41	0.48	1.24	0.985	−0.336
1.095	0.37	1.57	26.2	4.37	0.45	1.18	1.339	−0.542

TABLE 1. Properties of three-dimensional cells at steady state

et al. (1978). The two latex particles on the membrane serve as Lagrangian markers. We expect that as s is increased, the computed shapes will approximate the photographed shapes with increasing accuracy. Note, however, that because the grid lines in the computations are convected with the normal velocity of the membrane, the contour lines do not represent actual particle paths.

In table 1 we summarize the computed cell aspect ratios and orientation, maximum tension, tank-treading frequency, effective shear stress, and normal stress differences at steady state. The aspect ratio A_{xy} is defined as the ratio of the maximum to minimum cell dimension in the (x, y)-plane. The apparent aspect ratio A^a_{xz} is defined as the ratio of the maximum to minimum dimension of the projection of the cell onto the (x, y)-plane. As s is increased, both aspect ratios become higher, indicating that the cell tends to become more deformed, whereas the orientation angle is reduced, indicating that the cell tends to align with the shear flow. As in the case of two-dimensional flow, higher sphericity implies lower maximum tension, lower effective shear stress, and higher first and second normal stress differences. As in the case of suspensions of liquid drops, the first normal stress difference $\mathcal{N}_1$ is positive whereas the second normal stress difference $\mathcal{N}_2$ is negative, and this suggests that a dilute suspension behaves like a non-Newtonian

fluid with some elastic properties similar to those exhibited by polymeric solutions (Schowalter 1978).

Focusing on the behaviour of the tank-treading frequency, we compare the results of table 1 for a three-dimensional cell to those in figure 6(*c*) for a two-dimensional cell with corresponding circularity, and find good agreement. This suggests that the tank-treading frequency is not sensitive to the finite size of the cell in the z-direction. In §3 we saw that the computed tank-treading frequency of two-dimensional cells agrees remarkably well with that observed for real blood cells. Hence, by extrapolation, the tank-treading frequency that would arise from the present three-dimensional model is expected to agree well with laboratory measurements for normal blood cells (Tran-Son-Tay *et al.* 1984).

The tank-treading frequencies shown in table 1 are computed using equation (21) with the time period T calculated from the tangential velocity around the trace of the membrane in the (x,y)-plane. Fischer *et al.* (1978) report that all points on the membrane tank-tread approximately with the same frequency, a feature that may be attributed to the membrane elasticity. To assess the consequences of neglecting the viscoelastic properties of the membrane on the variation of the membrane tank-treading frequency f over the cell surface, we calculate f following a marker point starting from a grid point off the (x,y)-plane when the cell has reached a steady state, and find that the variation in the tank-treading frequency is not significant. For instance, for $s = 1.031$, when the marker point starts from the third, fifth, and seventh η-line along the first ξ-line, f/k is equal to 0.495, 0.500, and 0.502, respectively, which is about 4% different from 0.48, the value shown in table 1.

5. Summary

We studied the transient and asymptotic deformation of two-dimensional and three-dimensional liquid capsules enclosed by incompressible membranes as a model of red blood cell deformation in simple shear flow. Assuming that the mechanical response of the membrane is dominated by isotropic tension and the viscosity of the cytoplasmic fluid is equal to that of the suspending medium, we considered the motion as a function of the cell circularity or sphericity expressing the reduced ratio of the membrane perimeter or surface area to the cell area or volume. The two-dimensional and three-dimensional evolutions showed many qualitative and, in some cases, quantitative similarities, and this suggests that the salient features of the cell deformation may be predicted or reduced from two-dimensional models.

At steady state the membrane rotates around the cell in a tank-treading model. The tank-treading frequency of a two-dimensional cell is close to that of a three-dimensional cell, and in good agreement with experimental observations of normal red blood cells. As the sphericity is increased, the effective shear stress of a dilute suspension decreases because the cell tends to align with the mean flow, therefore reducing the rate of viscous dissipation within the fluid. The magnitude of the normal stress differences increases as the cell becomes more deformed, thereby introducing a higher degree of anisotropy to the flow. A dilute suspension of red cells is expected to behave like an elastic fluid.

The authors wish to acknowlege Dr Xiaofan Li for valuable discussions and the referees for constructive comments. This research is supported by the National Science Foundation under grant CTS-9216176, the Department of Energy under grant DE-FG03-94ER25192, and the Exxon Education Foundation.

REFERENCES

BARTHÈS-BIESEL, D. 1980 Motion of a spherical microcapsule freely suspended in a linear shear flow. *J. Fluid Mech.* **100**, 831–853.

BARTHÈS-BIESEL, D. & RALLISON, J. M. 1981 The time-dependent deformation of a capsule freely suspended in a linear shear flow. *J. Fluid Mech.* **113**, 251–267.

BARTHÈS-BIESEL, D. & SGAIER, H. 1985 Role of membrane viscosity in the orientation and deformation of a spherical capsule suspended in shear flow. *J. Fluid Mech.* **160**, 119–135.

BEISSINGER, R. L. & LAUGEL, J.-F. 1987 Low-stress hemolysis in laminar blood flow: Bulk and surface effects in capillaries. *AIChE J.* **33**, 99–108.

BRENNEN, C. 1975 A concentrated suspension model for the Couette rheology of blood. *Can. J. Chem. Engng* **53**, 126–133.

DINTENFASS, L. 1962 Considerations of the internal viscosity of red cells and its effect on the viscosity of whole blood. *Angiology* **13**, 333–344.

EVANS, E. A. & FUNG, Y. C. 1972 Improved measurements of the erythrocyte geometry. *Microvasc. Res.* **4**, 335–347.

EVANS, E. A. & HOCHMUTH, R. M. 1976 Membrane viscoelasticity. *Biophys. J.* **16**, 1–11.

EVANS, E. A. & SKALAK, R. 1980 *Mechanics and Thermodynamics of Biomembranes.* CRC Press.

FISCHER, T. M. 1980 On the energy dissipation in a tank-treading human red blood cell. *Biophys. J.* **32**, 863–868.

FISCHER, T. M. 1992 Is the surface area of the red cell membrane skeleton locally conserved? *Biophys. J.* **61**, 298–305.

FISCHER, T. M., STÖHR-LIESEN, M. & SCHMID-SCHÖNBEIN, H. 1978 The red cell as a fluid droplet: Tank tread-like motion of the human erythrocyte membrane in shear flow. *Science* **202**, 894–896.

GOLDSMITH, H. L. 1971 Deformation of human red cells in tube flow. *Biorheology* **7**, 235–242.

GOLDSMITH, H. L. & MARLOW, J. 1972 Flow behavior of erythrocytes. I. Rotation and deformation in dilute suspensions. *Proc. R. Soc. Lond.* B **182**, 351–384.

KELLER, S. R. & SKALAK, R. 1982 Motion of a tank-treading ellipsoidal particle in a shear flow. *J. Fluid Mech.* **120**, 27–47.

KENNEDY, M. R., POZRIKIDIS, C. & SKALAK, R. 1994 Motion and deformation of liquid drops and the rheology of dilute emulsions in simple shear flow. *Computers and Fluids* **23**, 251–278.

KHOLEIF, I. A. & WEYMANN, H. D. 1974 Motion of a single red blood cell in plane shear flow. *Biorheology* **11**, 337–348.

KRASNY, R. 1986 A study of singularity formation in a vortex sheet by the point-vortex approximation. *J. Fluid Mech.* **167**, 65–93.

LI, X. Z., BARTHÈS-BIESEL, D. & HELMY, A. 1988 Large deformations and burst of a capsule freely suspended in an elongational flow. *J. Fluid Mech.* **187**, 179–196.

LONGUET-HIGGINS, M. S. & COKELET, E. D. 1976 The deformation of steep surface waves on water I. A numerical method of computation. *Proc. R. Soc. Lond.* A **350**, 1–26.

NIIMI, H. & SUGIHARA, M. 1985 Cyclic loading on the red cell membrane in a shear flow: a possible cause of hemolysis. *J. Biomech. Engng* **107**, 91–95.

POZRIKIDIS, C. 1990 The axisymmetric deformation of a red blood cell in uniaxial straining Stokes flow. *J. Fluid Mech.* **216**, 231–254.

POZRIKIDIS, C. 1992 *Boundary Integral and Singularity Methods for Linearized Viscous Flow.* Cambridge University Press.

POZRIKIDIS, C. 1993 On the transient motion of ordered suspensions of liquid drops. *J. Fluid Mech.* **246**, 301–320.

POZRIKIDIS, C. 1994 Effects of surface viscosity on the finite deformation of liquid drops and the rheology of dilute emulsions in simple shearing flow. *J. Non-Newtonian Fluid Mech.* **51**, 161–178.

POZRIKIDIS, C. 1995 Finite deformation of liquid capsules enclosed by elastic membranes in simple shear flow. Submitted.

RICHARDSON, E. 1974 Deformation and haemolysis of red cells in shear flow. *Proc. R. Soc. Lond.* A **338**, 129–153.

RICHARDSON, E. 1975 Applications of a theoretical model for haemolysis in shear flow. *Biorheology* **12**, 27–37.

SCHMID-SCHÖNBEIN, H. & WELLS, R. E. 1969 Fluid drop like transition of erythrocytes under shear stress. *Science* **165**, 288–291.

SCHOWALTER, W. R. 1978 *Mechanics of Non-Newtonia Fluids*. Pergamon Press.

SKALAK, R., ÖZKAYA, N. & SKALAK, T. C. 1989 Biofluid mechanics. *Ann. Rev. Fluid Mech.* **21**, 167–204.

STONE, H. 1994 Dynamics of drop deformation and breakup of viscous fluids. *Ann. Rev. Fluid Mech.* **26**, 65–102.

SUGIHARA, M. & NIIMI, H. 1984 Numerical approach to the motion of a red blood cell in Couette flow. *Biorheology* **21**, 734–749.

SUTERA, S. P. & KROGSTAD, D. J. 1991 Reduction of the surface-volume ratio: a physical mechanism contributing to the loss of red cell deformability in malaria. *Biorheology* **28**, 221–229.

SUTERA, S. P. & MEHRARDI, M. H. 1975 Deformation and fragmentation of human red blood cells in turbulent shear flow. *Biophys. J.* **15**, 1–10.

SUTERA, S. P., MUELLER, E. R. & ZAHALAK, G. I. 1990 Extensional recovery of an intact erythrocyte from a tank-treading motion. *J. Biomech. Engng* **112**, 250–256.

SUTERA, S. P., PIERRE, P. R. & ZAHALAK, G. I. 1989 Deduction of intrinsic mechanical properties of the erythrocyte membrane from observations of tank-treading in the rheoscope. *Biorheology* **26**, 177–197.

TÖZEREN, A., SKALAK, R., FEDORCIW, B., SUNG, K. L. P. & CHIEN, S. 1984 Constitutive equations of erythrocyte membrane incorporating evolving preferred configuration. *Biophys. J.* **45**, 541–549.

TRAN-SON-TAY, R., SUTERA, S. P. & RAO, P. R. 1984 Determination of red blood cell membrane viscosity from rheoscopic observations of tank-treading motion. *Biophys. J.* **46**, 65–72.

ZAHALAK, G. I., RAO, P. R. & SUTERA, S. P. 1987 Large deformations of a cylindrical liquid-filled membrane by a viscous shear flow. *J. Fluid Mech.* **179**, 283–305.

ZHOU, H. & POZRIKIDIS, C. 1993*a* The flow of suspensions in channels: single files of drops. *Phys. Fluids* A **5**, 311–324.

ZHOU, H. & POZRIKIDIS, C. 1993*b* The flow of ordered and random suspensions of two-dimensional drops in a channel. *J. Fluid Mech.* **255**, 103–127.